Biennial Variability in an Atmospheric General Circulation Model

MICHAEL A. ALEXANDER

Cooperative Institute for Research in Environmental Sciences, University of Colorado, Boulder, Colorado

KLAUS M. WEICKMANN

Climate Diagnostic Center/NOAA, Boulder, Colorado

ABSTRACT

Recent observational analyses have indicated that tropospheric quasi-biennial oscillations (QBs) may play a fundamental role in regulating the timing and strength of El Niño and the Southern Oscillation. The biennial variability is examined in the tropical troposphere of a 35-year general circulation model (GCM) simulation forced by observed sea surface temperatures (SSTs). The results of spectral analyses and temporal filtering applied to the SST boundary conditions and the simulated lower- and upper-tropospheric zonal winds, precipitation, and sea level pressure anomalies are compared with observations and used to investigate the relationship between variables.

The GCM obtains regions of coherent biennial variability over the tropical Indian and Pacific Oceans in close correspondence with observations. In addition, the evolution of the stronger QBs and the physical relationship between variables are fairly well simulated. Zonal wind anomalies, with a simple baroclinic structure, tend to propagate eastward from the Indonesian region to the central Pacific where they increase in strength. The amplitude of the zonal wind and SST anomalies in the central Pacific vary together, with the largest anomalies occurring during the mid-1960s, mid-1970s, and early 1980s. During the time of the warmest SSTs, low pressure is found in the east Pacific with high pressure over Indonesia, and precipitation is enhanced between the date line and 120°W. However, the model underestimates the low-frequency variability in general and has approximately one-half to two-thirds of the observed variability in the biennial range. In addition, the observed phasing of the biennial and annual cycles in the zonal winds over the eastern Indian Ocean is not reproduced by the model.

The authors have also compared the amount of biennial variability of the near-surface zonal winds in the 35-year run with observed SSTs to two 35-year periods in a 100-year control run with climatological SSTs that repeat the seasonal cycle. Only the simulation with observed SSTs has an organized region of enhanced biennial variability near the equator, suggesting a strong oceanic component to the forcing of the QB.

1. Introduction

Fluctuations on approximately 2-year timescales, quasi-biennial oscillations, have been noted in climate records over many different parts of the earth as far back as the late 1800s [see Landsberg (1962)]. Quasi-biennial oscillations are contained in observations of air temperature, sea level pressure (SLP), sea surface temperature (SST), precipitation, etc. [e.g., Landsberg et al. (1963); Trenberth (1975, 1980); Meehl (1987); Kawamura (1988); Lau and Sheu (1988)]. A quasi-biennial oscillation (QBO) is also very prominent in the tropical stratospheric winds (Reed et al. 1961; Naujokat 1986). The stratospheric QBO appears to be caused by the vertical transfer of momentum by equatorial Kelvin and Rossby gravity waves [cf. Lindzen

and Holten (1968); Andrews et al. (1987)]. Yasunari (1989), Angell (1992), and Gray et al. (1992) found evidence of a link between the tropospheric and stratospheric biennial oscillations, while Trenberth (1980), Barnett (1991), and Xu (1992) have concluded that they are independent phenomena. Thus, the cause(s) of the quasi-biennial fluctuations in the tropical troposphere, referred to as QB from here on, and their relationship with oscillations in other parts of the globe remain unclear.

The dominant mode of variability on interannual timescales in the Tropics is associated with El Niño and the Southern Oscillation (ENSO). The Southern Oscillation (SO), the atmospheric component of ENSO, contains an SLP anomaly pattern with centers of opposite sign on either side of the tropical Pacific. Biennial variability in the SO was first noted by Berlage (1956, 1957). More recent studies indicate the SO has a range of approximately 2–10 years with a peak at 3–6 years (Trenberth 1976; Julian and Chervin 1978). However, a distinct secondary peak with an approxi-

Corresponding author address: Dr. Michael A. Alexander, University of Colorado, CIRES, Campus Box 449, Boulder, CO 80309-0449.

mately 2–3-year period has been noted in some SO indices (Rasmusson and Carpenter 1982; Keppenne and Ghil 1992). Composites of El Niño events indicate that warming of the ocean in the equatorial Pacific and the associated atmospheric changes over the globe evolve over about a 2-year period (Rasmusson and Carpenter 1982; van Loon and Shea 1985; Kiladis and Diaz 1989). Yasunari (1985) and Gutzler and Harrison (1987) found that the biennial oscillation interacts with a lower-frequency oscillation (4–5 year) to regulate the timing and strength of ENSO. Recent diagnostic analyses by Rasmusson et al. (1990), Barnett (1991), Ropelewski et al. (1992), and Jiang et al. (1993) appear to confirm that the tropospheric quasi-biennial tendency is an independent and statistically significant mode of ENSO.

The aforementioned studies plus many others provide a general description of the QB in the tropical troposphere. Like other low-frequency modes in the Tropics, the QB has a baroclinic structure with wind anomalies of opposite sign in the lower and upper levels of the troposphere, and it is composed of low horizontal wavenumbers indicative of large spatial scales. The QB is largest along the equatorial band over much of the Indian and Pacific Oceans and in the subtropical western Pacific in the Southern Hemisphere. Zonal wind anomalies tend to propagate from about 100°E to 150°W, but there is also a standing component with opposite anomalies over the Indian and central Pacific Oceans. The timing and strength of the QB varies; for example, the biennial signal was strong and fairly regular between 1968 and 1975, but a phase shift occurred in 1970 and the magnitude of the anomalies became weak in the late 1970s. Although the period of the QB is not strictly 2 years, there is a tendency for the minimum (maximum) amplitude of the surface wind on biennial timescales to occur in spring (fall) over the eastern Indian Ocean, indicating that the oscillations are loosely phased with the annual cycle.

There are also changes in the tropical ocean that appear to be closely related to the tropospheric QB. Coherent SST anomalies, which fluctuate on approximately 2-year timescales, are found in the Indian and Pacific Oceans. The largest SST anomalies, located in the central and east Pacific, tend to occur when the biennial zonal-wind anomalies are at a maximum in the central Pacific. Kawamura (1988) and Meehl (1993) showed that the QB surface temperature anomalies extend down into the ocean reaching depths of over 150 m and that these anomalies can persist for a year or more.

Trenberth (1975), Brier (1978), Nicholls (1978, 1979), and Hackert and Hastenrath (1986) suggested that air–sea interaction may play a fundamental role in the tropical tropospheric QB. Nicholls (1979) used a conceptual model to explain the QB. The model involves local air–sea interactions in the Indonesia–New Guinea area that depend on the season. Meehl (1987, 1993) expanded on Nicholls's ideas to include thermodynamic air–sea interaction along the entire belt traversed by the major center of convection in the Indian/west Pacific Oceans over the course of a year. The basic mechanism includes a westward shift in convection in one year, which causes cold ocean temperatures through locally enhanced surface fluxes and vertical mixing, resulting in an eastward shift in convection in the following year. Other biennial mechanisms involving a dynamical ocean component have been proposed by Kawamura (1988) and Münnich et al. (1991).

General circulation models (GCMs) have been used only recently to examine biennial variability in the tropical troposphere. Latif et al. (1993) found that the second largest mode of variability in a coupled atmosphere–ocean GCM simulation had a period of about 2 years. The SST anomalies associated with this mode in the model bear some resemblance to those in the data albeit with a slightly shorter period, but the zonal surface wind anomalies propagate westward, in contrast to observations. Some of the model data differences may result from errors in the model climatology, particularly the absence of warm water in the western equatorial Pacific. Robertson et al. (1993) also identified a quasi-biennial signal in a coupled GCM simulation, but the oscillation was weak and appeared to decay with time as the simulation progressed.

In this study, the atmospheric circulation is examined in extended atmospheric GCM simulations, described in section 2. We have two primary goals: (i) to examine the role of SST anomalies in the QB by comparing a GCM run with observed SST boundary conditions to a control run, where the SSTs repeat the same climatological seasonal cycle (section 3), and (ii) to test the model's ability to simulate the observed atmospheric characteristics of the QB in the run with observed SSTs (section 4). The results are discussed and summarized in section 5.

2. Atmospheric GCM and experiment design

The GCM used in this study is a global primitive equation model developed at the Geophysical Fluid Dynamics Laboratory (GFDL). It is a spectral model with rhomboidal truncation at wavenumber 15, a horizontal resolution of approximately 4.5° lat × 7.5° long. The vertical domain of the model is divided into nine unequal sigma (σ) layers where the lowest level, $\sigma = 0.991$, is approximately 50 m above the surface. Insolation at the top of the atmosphere varies with the seasons but has a fixed value during each day. The land surface temperature is computed assuming an instantaneous energy balance, while soil moisture is predicted using the bucket method. Large-scale precipitation occurs when the air column becomes saturated, while subgrid-scale precipitation is parameterized via convective adjustment. Other physical processes include
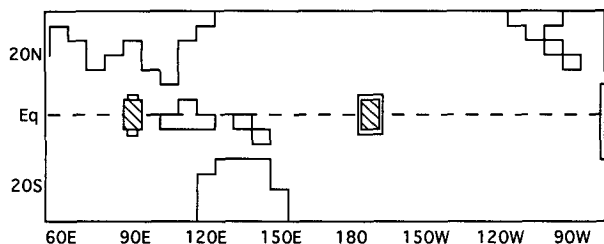
FIG. 1. Map of the GFDL GCM configuration over the tropical Indian and Pacific Ocean regions. Simulated (observed) area-averaged values are computed for the hatched (open) boxes located on the equator at 90°E and 172.5°W.

variable sea ice and continental snow cover, ice-albedo feedback, and radiative transfer. The model is described in more detail by Manabe and Hahn (1981) and Lau (1981) and has been used by Keshavamurty (1982) and Lau (1985) to study the atmospheric response to SST anomalies in the tropical Pacific associated with ENSO.

In the present study, we analyze an extended GFDL GCM simulation originally performed by Lau and Nath (1990). They evaluated the relative influence of tropical and midlatitude SST anomalies on the mid-latitude atmospheric circulation in a simulation where observed SSTs were prescribed at all ocean points between 60°N and 38°S, while climatological SSTs were specified over the remainder of the oceans. The simulation is 35-years long, extending from January 1950 to December 1984. We will examine this "global ocean–global atmosphere" (GOGA) experiment, focusing on the tropical Indian and Pacific sectors (Fig. 1), where the QB is strongest. The results from the GOGA simulation are compared with a 100-yr control run where the prescribed SSTs repeat the mean seasonal cycle during each year of the experiment.

The two primary methods used to study the QB in the model and in observed time series obtained from the Comprehensive Ocean–Atmosphere Data Set (COADS) are spectral analyses and temporal filtering. These methods are applied to monthly anomalies, which are obtained by subtracting the 35-yr average of each month from the corresponding month of the individual years. The spectral analyses include variance spectra of regionally averaged variables and the coherence and phase in the biennial range of model variables at grid points in the Tropics with an SST time series in the equatorial east Pacific. Irregular oscillations in the time series may cause power from other frequencies to leak into the biennial band in the analyzed spectra, as a result of discrete Fourier transforms. In additional analyses, the monthly anomalies are time filtered using a recursive Butterworth filter described by Murakami (1979), which has a maximum response at 25 months with the half-power points at 18 and 32 months.

3. The influence of SST anomalies on biennial variability

Evidence for enhanced biennial variability due to the prescribed SST anomalies is obtained by comparing the GOGA and control simulations. The three panels in Fig. 2 show the percentage of the monthly variability of the zonal wind anomalies in the biennial band: the top panel is from the 35-yr GOGA run, while the bottom panels are obtained from two separate 35-yr periods in the 100-yr control run. In the GOGA run, the variance in the biennial band exceeds 5% in the eastern Indian Ocean and across the entire tropical Pacific, with a maximum of slightly more than 10% on the equator at 110°W. While only a modest amount of the variability falls in the biennial range in the GOGA simulation, the two periods from the control run show no organized region of enhanced variability near the equator. This indicates that the SST anomalies and thus air–sea interactions likely play an important role in forcing the QB. It is possible that some of the variability in the biennial range in the control run results from the inclusion of interactive soil moisture that tends to enhance a broad spectrum of low-frequency variability (T. Delworth 1993, personal communication).

Ropelewski et al. (1992) examined the percent variability of the zonal wind in the biennial range relative to the total variance (which includes the annual cycle) rather than the anomalous monthly variance. We have performed a similar analysis using the GOGA run (not shown) and the agreement between the model and observations in terms of the location of enhanced QB variability is reasonably good. Both have regions of relatively high variability along the equator in the central and west Pacific and in the east Indian Ocean. However, the percent of the total monthly variance in the biennial range is roughly half as large in the GOGA
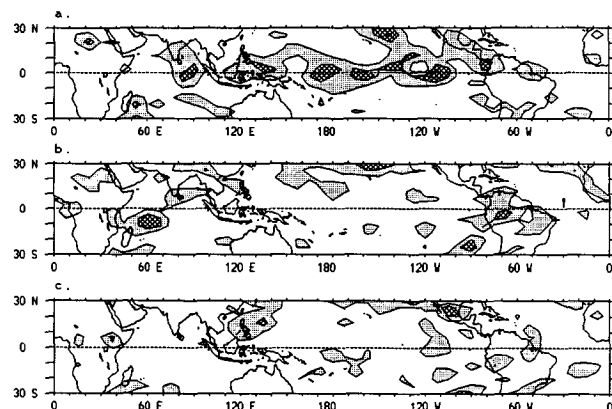

FIG. 2. The percent of the monthly anomalous variance of the near-surface u field in the biennial range in (a) the 35-year GOGA run with observed SSTs and (b) and (c) in two separate 35-year periods of a 100-year control run with climatological SSTs. Values exceeding 5% are shaded and values exceeding 7.5% are hatched.

run compared with observations: the maximum variance in the QB band is approximately 15% in nature and 7.5% in the model. This difference is also evident in individual spectra shown in section 4.

It should be noted that clouds in the control run were predicted, while they were specified by latitude and height in the GOGA run. While this difference will clearly influence many aspects of the simulated climate, variability in cloudiness did not appear to introduce an enhanced biennial signal in the atmospheric circulation, at least as indicated by the near-surface zonal winds (Figs. 2b, c). The difference between the GOGA and control simulations will be examined further in section 5.

4. Quasi-biennial variability in the GOGA simulation

The data analyses of Rasmusson et al. (1990) indicate that the QB signal is well defined in the SSTs in the central-east Pacific (170°E–90°W) and in the zonal component of the equatorial surface winds over the eastern Indian Ocean (70°–100°E) and the west-central Pacific (150°E–160°W). Hovmöller diagrams of the biennially filtered SST and u anomalies averaged over the grid points located at 2.2°N and 2.2°S for longitudes between 60°E and 82.5°W are shown in Fig. 3. The observed SST anomalies are largest in the Pacific Ocean between the date line and 90°W and sometimes exceed 1°C in the vicinity of 135°W. Smaller SST anomalies, on the order of 0.2°C, occur in the Indonesian region (surface temperatures from land points have been excluded between 105° and 135°E). In the eastern Pacific, the slight slope of the contours from upper right to lower left indicates westward propagation of the anomalies from the South American coast toward the date line. During the 1950s, the anomalies show some hint of eastward propagation from the west to the central Pacific; however, the anomaly pattern during this period is suspect due to the limited amount of data. In the early 1980s, the QB SST anomalies developed in the central Pacific and moved east; these biennial anomalies phased with lower-frequency anomalies (Barnett 1991; Ropelewski et al. 1992) to produce the major 1982 El Niño event. The SST anomalies contain periods of large-amplitude biennial fluctuations—from 1962 to 1966, from 1972 to 1976, and from 1982 to the end of the record—but as noted by Barnett (1991), the largest biennial fluctuations did not occur during the 1982/83 El Niño.

The simulated biennially filtered zonal wind anomalies (Fig. 3b) have maximum amplitude in the west-central Pacific (150°E–150°W), and sizable anomalies are also found between 70°–100°E and 115°–135°E with a node in between. In some instances, the u anomalies begin at around 115°E and propagate eastward into the Pacific where they increase in strength, exceeding $|0.6|$ m s^{-1} near the date line when the QB

is strong. Although noisier than the QB SST field, the u anomalies are generally stronger to the west of the maximum SST anomalies. The two fields tend to vary together with anomalous westerlies (positive u) associated with warmer water (positive SSTs) in the central Pacific and the east Indian Ocean. The magnitude of the zonal wind anomalies in the central Pacific and the SST anomalies in the east Pacific are generally largest during the same periods: the mid-1960s, mid-1970s, and early 1980s, in agreement with a similar analysis of the data by Ropelewski et al. (1992).

During some periods the wind anomalies have a dipole structure with anomalies of one sign in the central Pacific and the opposite sign in the Indian Ocean (Fig. 3b). For example, in the later part of 1963, anomalous westerlies are found in the vicinity of the date line, while anomalous easterlies are located from 140°E to the western edge of the domain. During the mid-1970s, the wind anomalies exhibited a three-cell structure with anomalies of one sign over the Indonesian sector flanked by anomalies of the opposite sign in the Indian and central Pacific Oceans. Ropelewski et al. (1992) found that the dipole pattern occurs most often in nature. The three-cell structure in the GCM may be related to the placement of land grid points in the model since the node in the u anomalies at 112.5°E occurs where land grid boxes are specified on either side of the equator (Fig. 1). An examination of a Hovmöller plot of the precipitation anomalies (not shown) indicates that enhanced precipitation tends to occur in regions of low-level zonal wind convergence located between positive u anomalies to the west and negative anomalies to the east.

The large-scale relationships between the simulated atmospheric variables in the Tropics and the observed SST boundary conditions in the central Pacific are examined further using cross-spectral analysis. The cross spectra between SST anomalies in the base region, 165°–112.5°W, 2.2°N–2.2°S, and (a) SST, (b) u at σ = .991, (c) u at σ = .205 ($\sim$200 mb), (d) SLP, and (e) precipitation anomalies between 30°N and 30°S are shown in Fig. 4. The coherent relationships in the biennial range centered on approximately 25 months are represented by harmonic dial vectors. The arrow direction denotes phase, while its length denotes the coherence squared. A vector pointing due north (south) indicates that the time series at that location is in (out of) phase with the SST in the base region, and a vector pointing due west (east) indicates that the time series leads (lags) the SST in the base region by approximately 6 months. Following Julian (1975), vectors are plotted only where the coherence squared exceeds the 90% confidence level or, equivalently, where the coherent variance accounts for more than 32% of the total variance in the biennial band.

Figure 4a indicates that the SST anomalies in a large region between 12°N and 12°S from the South American coast to the date line are coherent and nearly in

GOGA – BIENNIAL FILTERED SST ANOMALY (C) 2.2N–2.2S

GOGA –BIENNIAL FILTERED U990 ANOMALY (M/SEC) 2.2N–2.2S
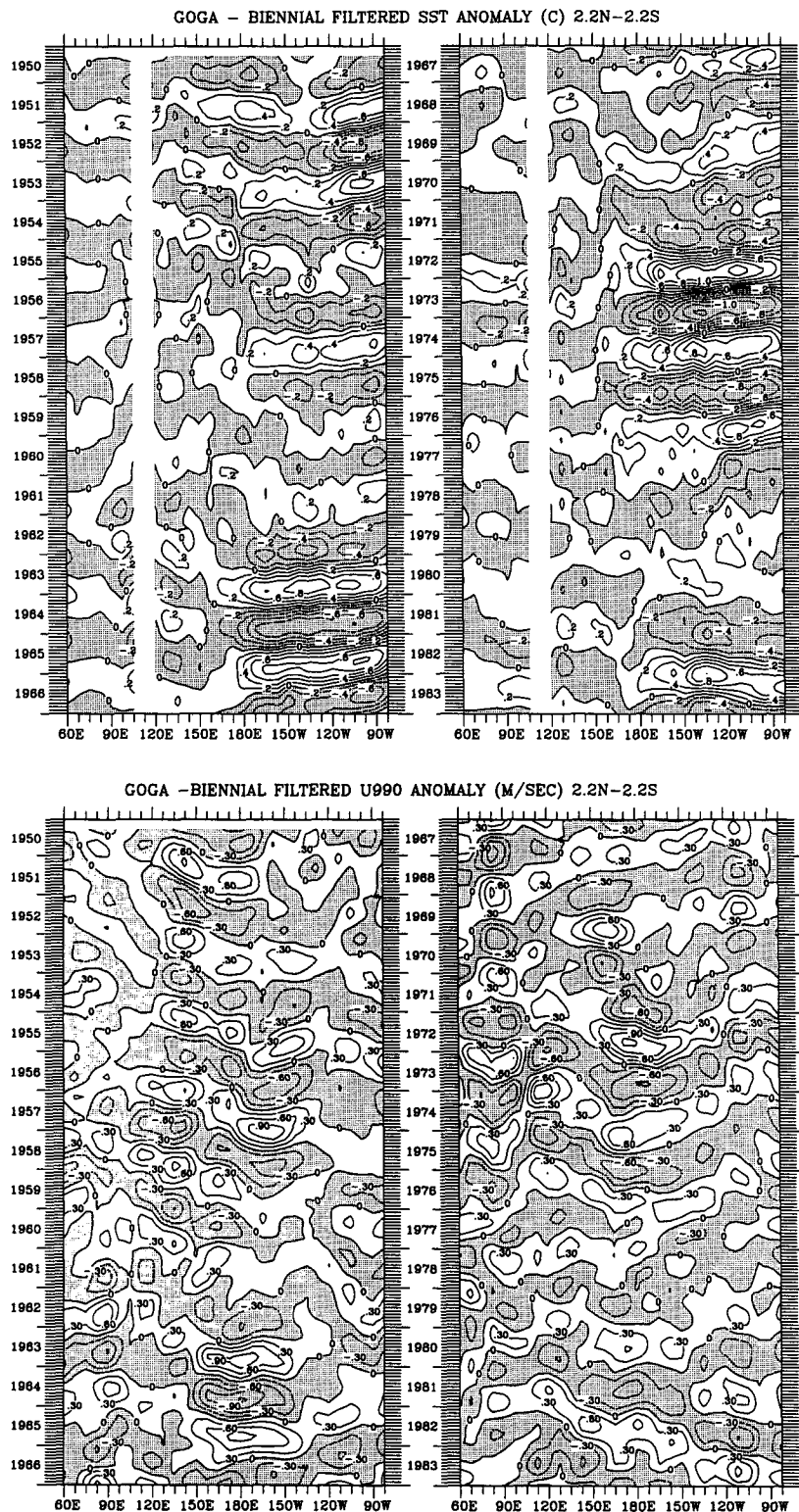
FIG. 3. Hovmöller plots of the biennial filtered (a) anomalous SSTs used as boundary conditions (°C) and (b) simulated near-surface u anomalies (m s^{-1}) between 60°E and 82.5°W averaged over the model grid points located at 2.2°N and 2.2°S. Negative values are shaded. Surface temperature values are excluded in (a) from land grid boxes in the Indonesian region (see Fig. 1), which includes both 2.2°N and 2.2°S at 112.5°E.
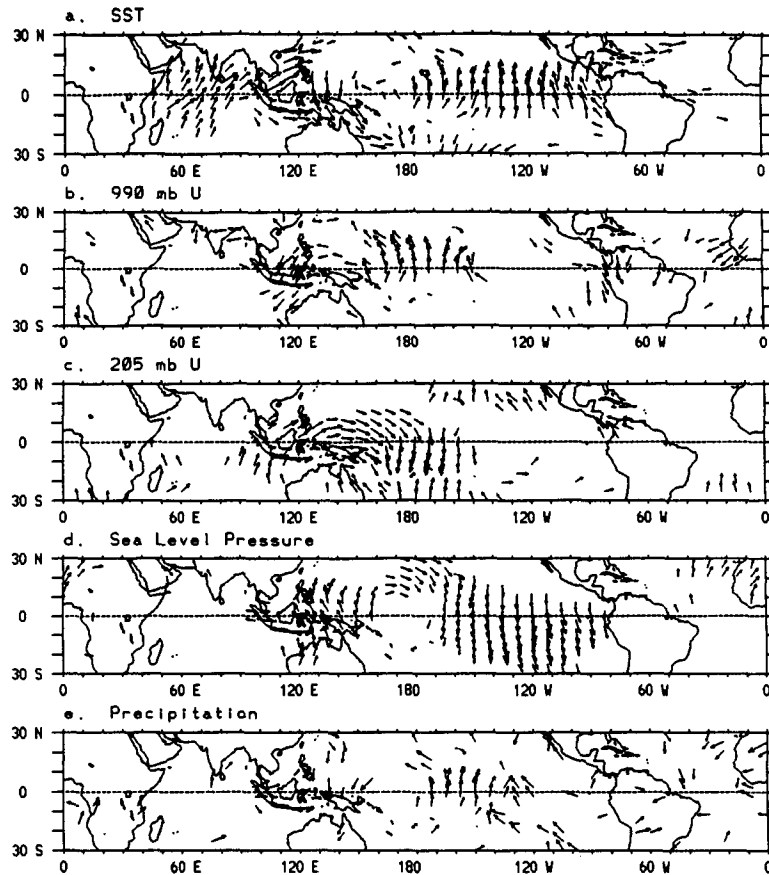
FIG. 4. Cross spectra, represented by harmonic dial vectors, between the SST in a base region, 2.2°N–2.2°S, 165°–112.5°W, and (a) SST, (b) u at σ = .991, (c) u at σ = .205, (d) SLP, and (e) precipitation at grid points over the global Tropics. The cross spectra are computed for biennial timescales, encompassing the band of approximately 21–30 months. The arrow direction denotes phase, while its length denotes the coherence squared. Vectors pointing due north (south) indicate the time series at that point is in (out of) phase with the SST time series in the base region, while those vectors that point east (west) lag (lead) the base time series by approximately 6 months. Only time series whose coherence squared is significant at the 90% level or, equivalently, that account for more than 32% of the variance in the 21–30-month band are plotted. The arrows are scaled by the maximum coherence squared for each variable: (a) 0.96, (b) 0.81, (c) 0.85, (d) 0.93, and (e) 0.81.

phase, though the clockwise turning of the vectors moving from 80°W toward 120°W implies westward propagation of the anomalies. The SST anomalies in the central Pacific lead those in the Indian Ocean by approximately 3 months and are out of phase with the anomalies near the Indonesian region as indicated by the vectors that point south. Coherent anomalies extend all the way from the eastern Indian Ocean, along the South Pacific convergence zone and to the subtropical south-central Pacific. The vectors rotate clockwise along this track, and the implied southeastward progression of SST anomalies may be related to alternating years of strong and weak monsoon circulations, as discussed by Meehl (1987, 1993).

The zonal component of the near-surface winds is coherent with the SST in the base region from 90°E

to 150°W (Fig. 4b). Clockwise rotation of the vectors within 15° of the equator from 90°E to the central Pacific implies eastward propagation of the zonal wind anomalies; eastward propagation is even more apparent in the upper-tropospheric winds (Fig. 4c). The low-level u anomalies near the date line and SST anomalies in the east Pacific (with a region of overlap between 180° and 150°W) are in phase, supporting the results from the Hovmöller diagrams. The orientation of the vectors in Fig. 4b and the domain over which they are coherent at the 90% level agrees well with the results of a cross-spectral analysis of observed u and SST anomalies in the biennial range by Ropelewski et al. (1992). One exception is that the coherent QB signal extends about 20° farther to the west over the Indian Ocean in nature. The vectors of the zonal-wind anom-

alies in the lower and upper troposphere are out of phase and thus oppose each other; this baroclinic structure is consistent with the observational studies of Yasunari (1985) and Gutzler and Harrison (1987). The dominant pattern in the SLP cross-spectra (Fig. 4d) is an out-of-phase relationship between two large regions, one over Indonesia and the other in the central and east Pacific. However, there is also a tendency for the SLP anomalies north of the equator to move eastward from about 130°E to 150°W. The SLP pattern from the GOGA run closely resembles the leading complex EOF of the biennially filtered observed SLP anomalies (Barnett 1991). The precipitation and SST anomalies tend to vary together in the central Pacific and north of New Guinea (Fig. 4e), although compared with the other model variables the precipitation anomalies exhibit a less coherent structure.

Viewed as a whole, Fig. 4 provides information about the interrelationships between the atmospheric variables and sea surface temperatures on approximately 2-year timescales. When SSTs are warmest in the central Pacific, anomalous westerlies occur near the surface in the western half of the Pacific basin with easterly anomalies above, low pressure is found in the east Pacific with high pressure over Indonesia, and precipitation is enhanced between the date line and 120°W. These conditions often occur during the height of an El Niño event in conjunction with the negative extreme of the Southern Oscillation. The close association between the SST boundary conditions and the simulated anomalies in the tropical troposphere on 2-yr timescales suggests that the ocean strongly influences the tropospheric QB.

Figures 2, 3b, 4b, and 4c indicate that enhanced biennial variability of the monthly zonal wind (u) anomalies extends from the east Indian Ocean to the central Pacific. A more detailed analyses of the QB in these two areas is obtained from power spectra of the u anomalies from the lowest model level at 90°E and at 172.5°W, averaging grid points values at 2.2°N and 2.2°S. In Fig. 5 spectra of the GOGA model winds are compared with observations from similar but not identical regions (see Fig. 1), as the GCM and COADS grids have different dimensions. Observed data were recorded for nearly all of the months in these two areas over the 35-year period; other regions of the Pacific had large data gaps, especially during the 1950s. The spectra at both locations indicate that the low-frequency variance, with periods of more than about 20 months, is greater in observations compared with the model (Fig. 5). This results in less total variance and reduced 1-month lag autocorrelation values in the model. In the eastern Indian Ocean (90°E), there is a prominent biennial peak that exceeds the 95% confidence level in the GCM but it explains approximately two-thirds the variance and has a maximum at a slightly lower frequency compared with the observed spectra. In addition, at 90°E the model does not contain the
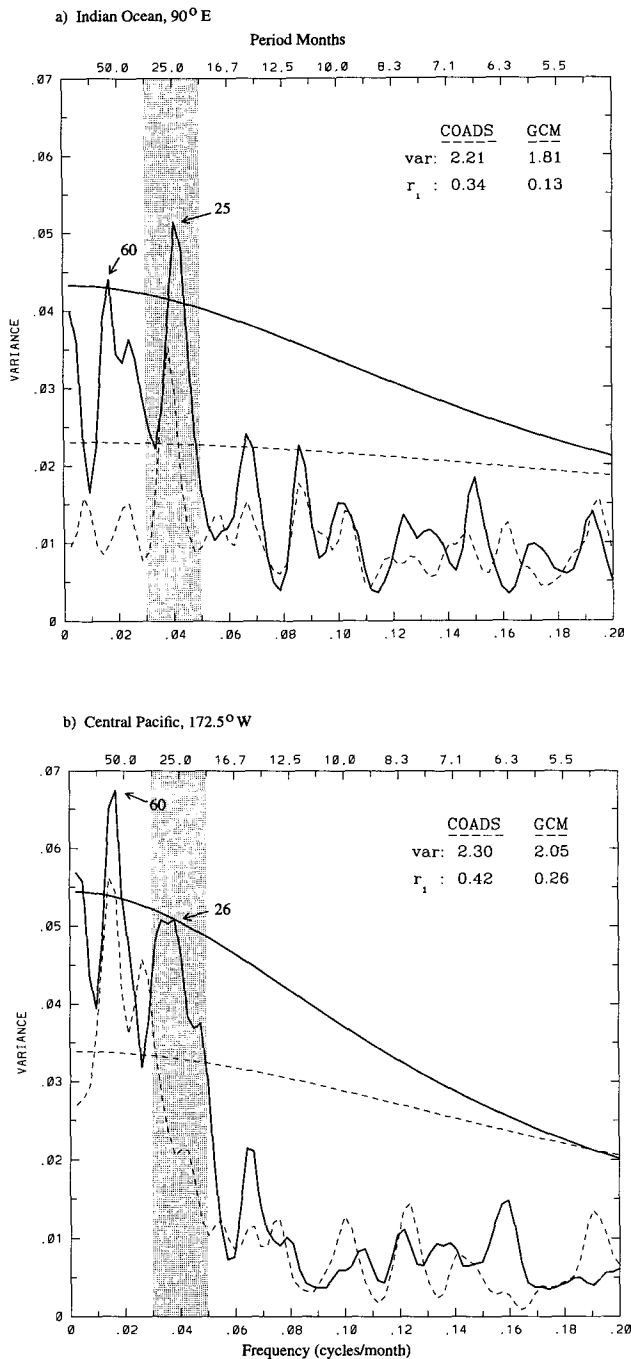

FIG. 5. Variance spectra of the zonal wind anomalies from the lowest GCM layer (dashed line) and from COADS (solid line) averaged over the regions shown in Fig. 1: (a) 90°E and (b) 172.5°W. Data are monthly anomalies from 1950 to 1984. Only the low-frequency portion of the spectrum is shown and the band between 20 and 33 months is shaded. The spectra are smoothed using three passes of a 1-2-1 filter. The 95% red-noise background spectrum, as determined from the lag 1 autocorrelation coefficient, is shown for the observed and simulated data by the smooth solid and dashed curves, respectively. The total variance (var) and 1-month lag autocorrelations (r_1) for the COADS and the GCM data are shown in the upper right-hand corner. The top abscissa is labeled with the period in months, while the bottom gives frequency in months^{-1}.

low-frequency ENSO component that has significant power between 3 and 6 yr in the observations. In contrast, in the central Pacific (172°W) both the model and observations have a significant low-frequency peak at about 60 months, but at 24 months the simulated variance is well below the 95% confidence level.

The QB in the tropical troposphere is further investigated by time filtering the near-surface model winds, retaining more than half of the power between 18 and 32 months. The filtered time series of the model zonal winds for the regions shown in Fig. 1, and the corresponding observed values from COADS are shown in Fig. 6.[1] The agreement between the observed and simulated time series is reasonably good; the two have a linear correlation of 0.54 at 90°E and 0.64 at 172.5°W. While it is difficult to estimate the degrees of freedom in the filtered time series, if we use a conservative estimate that there are 16 independent 26-month periods, the corresponding correlation value at the 95% significance level is 0.47, indicating that both correlation values are statistically significant. Both the simulated and observed time series contain prominent low-frequency modulation of the amplitude of the biennial filtered zonal wind: at 90°E the signal is strongest between 1960 and 1975; while at 172.5°W the signal is greatest in the mid-1960s and mid-1970s. On average, the amplitude of the quasi-biennial u anomalies in the model are roughly three-quarters to four-fifths as large as in the data; the simulated (observed) standard deviation of u is 0.44 (0.54) m s^{-1} at 90°E and 0.40 (0.54) m s^{-1} at 172.5°W. The general impression from Fig. 6 is that the model performs better when the observed biennial filtered u anomalies are large; that is, when $|u|$ exceeds approximately 0.5 m s^{-1}. The model does not reproduce the large swings in u at 90°E during the early 1950s and also underestimates u at 172.5°W during the early 1980s. The simulation in the 1950s is hampered by a lack of SST observations over much of the Pacific, and thus, the boundary conditions driving the model may not be representative of the true ocean state.

5. Discussion and conclusions

Many observational analyses (c.f. Rasmusson et al. 1990; Barnett 1991; Ropelewski et al. 1992) and some recent coupled atmosphere–ocean GCM experiments (Latif et al. 1993; Robertson et al. 1993) have found evidence of a quasi-biennial oscillation in the tropical troposphere that appears to play an important role in the evolution of El Niño and the Southern Oscillation. In this study, we have examined the variability in the biennial range in a 35-yr (1950–84) atmospheric GCM simulation forced with observed SSTs as boundary
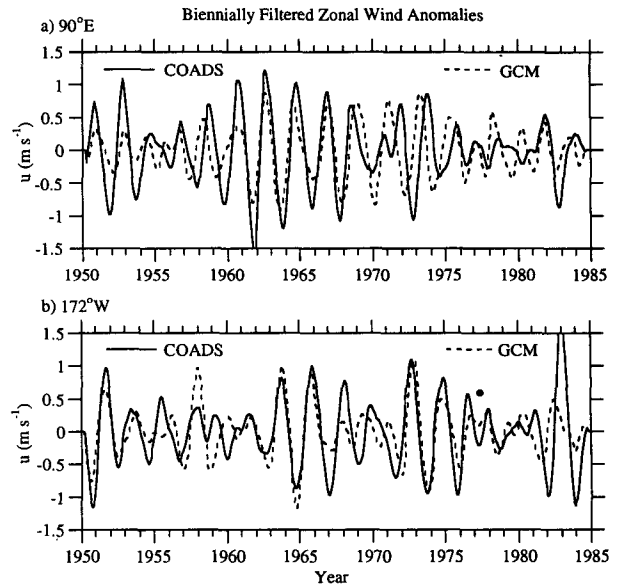
---

[1] The biennially filtered time series of the simulated zonal wind at 90°E obtained using singular spectrum analysis (Vautard and Ghil 1989) closely resembles the filtered time series shown in Fig 6a.

FIG. 6. Time series of the biennial filtered near-surface zonal wind u anomalies (m s^{-1}) from the model and from COADS for the same regions used in Fig. 1, located at (a) 90°E and (b) 172.5°W.

conditions. The results are compared with observations as a means to test the GCM's ability to resolve interannual climatic variability; the fidelity of the model on biennial timescales has implications for future model sensitivity and prediction experiments.

The model reproduces several aspects of the observed QB but has difficulty simulating others. The GCM performs well on biennial timescales in that (a) the regions of enhanced atmospheric variability are located in the tropical Indian and Pacific Oceans in close correspondence with observations; (b) time series of regional near-surface zonal wind anomalies u in the model and data are in reasonable agreement, and the correlation between the two are statistically significant, exceeding 0.54 over the east Indian Ocean and 0.64 in the central Pacific; (c) the u anomalies, which have opposite signs in the lower and upper troposphere, tend to propagate eastward from the Indonesian region to the central Pacific where they increase in strength; and (d) the amplitude of the u and SST anomalies vary together, with the largest anomalies occurring during the mid-1960s and 1970s and in the early 1980s. However, some aspects of the near-surface zonal wind field are not well simulated, in that: (a) the model generally underestimates the low-frequency variability and has approximately one-half to two-thirds of the observed variance in the biennial range; (b) spectral peaks on biennial timescales (2–3 yr) at 170°W and on timescales between ENSO events (3–7 yr) at 90°E are absent in the GCM; and (c) over the east Indian Ocean the model is unable to reproduce the phasing of QB fluctuations in u with the seasonal cycle found in observations (not shown).

If atmosphere–ocean interaction strongly influences the QB in the tropical troposphere, then the biennial signal should be contained in the SST anomalies. We have compared the amount of variability in the biennial range in the 35-yr run with observed SSTs to two 35-yr periods in a 100-yr control run with climatological SSTs that repeat the seasonal cycle. The simulation with observed SSTs has enhanced biennial variability of the surface zonal winds over much of the equatorial Pacific and Indian Oceans, while both periods from the control run have minimal biennial variance in these regions.

The conclusions drawn from the comparison between the GOGA and control simulations are influenced by two factors. 1) The two runs have different cloud parameterizations; the clouds are specified in the GOGA run but predicted by moist convective adjustment and layer saturation in the control run. 2) A single realization over the 35-yr period may not be representative of the model's mean response to the SST anomalies; a set of runs may be necessary to obtain stable statistics. We recently obtained the upper-level winds from a new set of four 43-yr GOGA simulations, extending from 1946 to 1988. These GOGA simulations have the same cloud parameterization as the 100-yr control simulation but differ only in their initial atmospheric states. Observational analysis by Yasunari (1985) and Gutzler and Harrison (1987) and the results from the original GOGA run (Fig. 4c) indicate a biennial signal in the upper-tropospheric zonal winds. The ensemble average of the percent variability in u at an approximate 200-mb level in the biennial band (21–30 months) from these four GOGA runs and two 43-yr periods in the control are shown in Fig. 7. An enhanced region of biennial variability is found in the GOGA composite centered over Indonesia and the central equatorial Pacific. While there is some variability among the GOGA simulations (not shown), all four had enhanced variability on biennial timescales in these regions. In contrast, the control run does not exhibit a coherent region of enhanced biennial variability within 20° of the equator.

The marked difference between the GOGA and control runs implies a strong oceanic component in the QB. We are not able to distinguish between the relative importance of SST anomalies in different regions in terms of their impact on the atmosphere. The largest SST anomalies located in the eastern equatorial Pacific are closely associated with the wind anomalies farther to the west near the date line. These anomalies are consistent with dynamically coupled atmosphere–ocean modes (cf. Hirst 1986; Battisti 1988; Philander 1990). From this standpoint, the key atmosphere–ocean interactions in the QB occur in the central equatorial Pacific. On the other hand, even though SST anomalies are small in the Indian Ocean and west Pacific, they may be important as they are superimposed on a warm base state. Observations and modeling
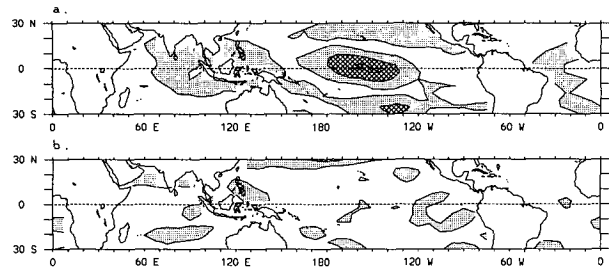

FIG. 7. The percent of the monthly anomalous variance of the u field in the biennial range at the $\sigma = 205$ from an ensemble of (a) four 43-yr GOGA runs and (b) two separate 43-yr periods of a 100-yr control run. As in Fig. 2, values exceeding 5% are shaded and values exceeding 7.5% are hatched.

studies have indicated that moisture convergence and convection are maximized over the warmest SSTs, not where the SST anomalies are largest (Ramage and Hori 1981; Graham and Barnett 1987; Philander 1990). Most of the studies concerning the role of the oceans in the QB have focused on thermodynamic air–sea interactions in the Indonesian and west Pacific regions (Trenberth 1975; Brier 1978; Nicholls 1978; 1979; Hackert and Hastenrath 1986; Meehl 1987, 1993). The biennial component of ENSO may involve complex interactions between the Asian and Indonesian monsoon regions, the Indian and Pacific Oceans, and the tropical atmosphere as suggested by the studies of Barnett (1983, 1984a,b, 1991), Rasmusson et al. (1990), and Ropelewski (1992).

REFERENCES

Andrews, D. G., J. R. Holton, and C. B. Leovy, 1987: *Middle Atmosphere Dynamics.* Academic Press, 489 pp.

Angell, J. K., 1992: Evidence of a relationship between El Niño and the QBO, for an El Niño in 1991–92. *Geophys. Res. Lett.,* **19,** 285–288.

Barnett, T. P., 1983: Interaction of the monsoon and Pacific trade wind system at interannual time scales. Part I: The equatorial band. *Mon. Wea. Rev.,* **111,** 756–773.

——, 1984a: Interaction of the monsoon and Pacific trade wind system at interannual time scales. Part II: The tropical band. *Mon. Wea. Rev.,* **112,** 2380–2387.

——, 1984b: Interaction of the monsoon and Pacific trade wind system at interannual time scales. Part III: A partial anatomy of the Southern Oscillation. *Mon. Wea. Rev.,* **112,** 2388–2400.

——, 1991: The interaction of multiple time scales in the tropical climate system. *J. Climate,* **4,** 269–285.

Battisti, D. S., 1988: The dynamics and thermodynamics of a warming event in a coupled tropical atmosphere–ocean model. *J. Atmos. Sci.,* **45,** 2889–2919.

Berlage, H. P., 1956: The Southern Oscillation, a 2–3 year fundamental oscillation of world-wide significance. *I.U.G.G. 10th General Assembly: Scientific Proc. of the Int. Association of Meteorology,* Rome, Italy, 336–345.

——, 1957: Fluctuations in the general atmospheric circulation of more than one year, their nature and prognostic value. *K. Ned. Meteor. Inst. Meded. Verh.,* **69,** 152 pp.

Brier, G. W., 1978: The quasi-biennial oscillation and feedback processes in the atmosphere-ocean-earth system. *Mon. Wea. Rev.,* **106,** 938–954.

Gray, W. M., J. D. Scheaffer, and J. A. Knaff, 1992: Influence of the stratospheric QBO on ENSO variability. *J. Meteor. Soc. Japan,* **70,** 975–995.

Gutzler, D. S., and D. E. Harrison, 1987: The structure and evolution of seasonal wind anomalies over the near-equatorial eastern Indian and western Pacific Oceans. *Mon. Wea. Rev.,* **114,** 285–294.

Hackert, E. C., and S. Hastenrath, 1986: Mechanisms of Java rainfall anomalies. *Mon. Wea. Rev.,* **114,** 745–757.

Hirst, A. C., 1986: Unstable and damped equatorial modes in simple coupled ocean–atmosphere models. *J. Atmos. Sci.,* **43,** 606–630.

Jiang, N., D. Neelin, and M. Ghil, 1993: Quasi-quadrennial and quasi-biennial variability in COADS equatorial sea-surface temperature and surface zonal winds. *Proc. 70th Annual Climate Diagnostic Workshop,* Norman, OK, U.S. Dept. of Commerce, 348–353.

Julian, P. R., 1975: Comments on the determination of significance levels of the coherence statistic. *J. Atmos. Sci.,* **32,** 836–837.

——, and R. M. Chervin, 1978: A study of the Southern Oscillation and the Walker circulation phenomenon. *Mon. Wea. Rev.,* **106,** 1433–1451.

Kawamura, R., 1988: Quasi-biennial oscillation modes appearing in the tropical sea water temperature and 700 mb zonal wind. *J. Meteor. Soc. Japan,* **66,** 955–965.

Keppenne, C., and M. Ghil, 1992: Adaptive filtering and prediction of the Southern Oscillation index. *J. Geophys. Res.,* **97,** 20 449–20 454.

Keshavamurty, R. N., 1982: Response of the atmosphere to sea surface temperature anomalies over the equatorial Pacific and the teleconnections of the Southern Oscillation. *J. Atmos. Sci.,* **39,** 1241–1259.

Kiladas, G. N., and H. F. Diaz, 1989: Global climatic anomalies associated with the extremes of the Southern Oscillation. *J. Climate,* **2,** 1069–1080.

Landsberg, H. E., 1962: Biennial pulses in the atmosphere. *Beitr. Phys. Atmos.,* **35,** 184–194.

——, J. M. Mitchell, Jr., H. L. Crutcher, and F. T. Quinlan: 1963: Surface signs of the biennial atmospheric pulse. *Mon. Wea. Rev.,* **101,** 549–556.

Latif, M., A. Sterl, E. Maier-Reimer, and M. M. Junge, 1993: Climate variability in a coupled GCM. Part I: The tropical Pacific. *J. Climate,* **6,** 5–21.

Lau, K.-M., and P. J. Sheu, 1988: Annual cycle, quasi-biennial oscillation and Southern Oscillation in global precipitation. *J. Geophys. Res.,* **93,** 10 975–10 988.

Lau, N.-C., 1981: A diagnostic study of recurrent meteorological anomalies appearing in a 15-year simulation with a GFDL general circulation model. *Mon. Wea. Rev.,* **109,** 2287–2311.

——, 1985: Modeling the seasonal dependence of the atmospheric response to observed El Niños in 1962–76. *Mon. Wea. Rev.,* **113,** 1970–1996.

——, and M. J. Nath, 1990: A general circulation model study of the atmospheric response to extratropical SST anomalies observed in 1950–79. *J. Climate,* **3,** 965–989.

Lindzen, R. S., and J. R. Holton, 1968: A theory of the quasi-biennial oscillation. *J. Atmos. Sci.,* **25,** 1095–1107.

Manabe, S., and D. G. Hahn, 1981: Simulation of atmospheric variability. *Mon. Wea. Rev.,* **109,** 2260–2286.

Meehl, G. A., 1987: The annual cycle and interannual variability in the tropical Pacific and Indian Ocean regions. *Mon. Wea. Rev.,* **115,** 27–50.

——, 1993: A coupled air–sea biennial mechanism in the tropical Indian and Pacific Regions: Role of the ocean. *J. Climate,* **6,** 31–41.

Münnich, M., M. A. Cane, and S. E. Zebiak, 1991: A study of self-excited oscillations of the tropical ocean–atmosphere system. Part II: Nonlinear cases. *J. Atmos. Sci.,* **48,** 1238–1248.

Murakami, M., 1979: Large-scale aspects of deep convective activity over the GATE area. *Mon. Wea. Rev.,* **107,** 994–1013.

Naujokat, B., 1986: An update of the observed quasi-biennial oscillation of the stratospheric winds over the Tropics. *J. Atmos. Sci.,* **43,** 1873–1877.

Nicholls, N., 1978: Air-sea interaction and the quasi-biennial oscillation. *Mon. Wea. Rev.,* **106,** 1505–1508.

——, 1979: A simple air-sea interaction model. *Quart. J. Roy. Meteor. Soc.,* **105,** 93–105.

Philander, S. J., 1990: *El Niño, La Niña, and the Southern Oscillation.* Academic Press, 293 pp.

Rasmusson, E. M., and T. H. Carpenter, 1982: Variations in the tropical sea surface temperature and surface wind fields associated with the Southern Oscillation/El Niño. *Mon. Wea. Rev.,* **110,** 354–384.

——, X. Wang, and C. F. Ropelewski, 1990: The biennial component of ENSO variability. *J. Mar. Sys.,* **1,** 71–90.

Reed, R. J., W. J. Campbell, L. A. Rasmussen, and D. G. Rogers, 1961: Evidence of downward-propagating annual wind reversal in the equatorial stratosphere. *J. Geophys. Res.,* **66,** 813–818.

Robertson, A. W., C.-C. Ma, C. R. Mechoso, and M. Ghil, 1993: Simulations of the tropical Pacific Climate with the UCLA coupled GCM. *Proc. 70th Annual Climate Diagnostic Workshop,* Norman, OK, U.S. Department of Commerce, 272–276.

Ropelewski, C. F., M. S. Halpert, and X. Wang, 1992: Observed tropospheric biennial variability and its relationship to the Southern Oscillation. *J. Climate,* **5,** 594–614.

Trenberth, K. E., 1975: A quasi-biennial standing wave in the Southern Hemisphere and interrelations with sea surface temperature. *Quart. J. Roy. Meteor. Soc.,* **101,** 55–74.

——, 1976: Spatial and temporal variations in the Southern Oscillation. *Quart. J. Roy. Meteor. Soc.,* **102,** 639–653.

——, 1980: Atmospheric quasi-biennial oscillations. *Mon. Wea. Rev.,* **108,** 1370–1377.

van Loon, H., and D. J. Shea, 1985: The Southern Oscillation. Part IV: The precursors south of 15°S to the extremes of the oscillation. *Mon. Wea. Rev.,* **113,** 2063–2074.

Vautard, R., and M. Ghil, 1989: Singular spectrum analysis in nonlinear dynamics, with applications to paleoclimatic timeseries. *Physica,* **35D,** 395–424.

Xu, J., 1992: On the relationship between the quasi-biennial oscillation and the tropospheric Southern Oscillation. *J. Atmos. Sci.,* **49,** 725–734.

Yasunari, T., 1985: Zonally propagating modes of the global east-west circulation associated with the Southern Oscillation. *J. Meteor. Soc. Japan,* **63,** 1013–1029.

——, 1989: A possible link of the QBOs between the stratosphere, troposphere and sea surface temperature in the Tropics. *J. Meteor. Soc. Japan,* **67,** 483–493.